Spring 2015

Hydrodynamics of Unitary Fermi Gases

Jasmine Brewer
Jasmine.Brewer@Colorado.EDU

Hydrodynamics of Unitary Fermi Gases

by

Jasmine Brewer

A thesis submitted to the

Faculty of the University of Colorado

in partial fulfillment of the

requirements for the degree of

Bachelor of Science

Department of Physics

2015

This thesis entitled:
Hydrodynamics of Unitary Fermi Gases
written by Jasmine Brewer
has been approved for the Department of Physics

Paul Romatschke

David Grant

Jun Ye

Date

The final copy of this thesis has been examined by the signatories, and we find that both the content and the form meet acceptable presentation standards of scholarly work in the above mentioned discipline.

Brewer, Jasmine (Engineering Physics)

Hydrodynamics of Unitary Fermi Gases

Thesis directed by Paul Romatschke

In this thesis we present fully nonlinear dissipative hydrodynamics simulations using the lattice Boltzmann method which we have developed to study hydrodynamics in cold atomic gases. We motivate and derive the specifics of the lattice Boltzmann implementation for this system, and then use our simulations to study collective oscillations in two-dimensional Fermi gases. We show that all dominant frequencies and damping rates of the breathing and quadrupole oscillatory modes agree quantitatively with analytic solutions in the hydrodynamic limit for a gas with ideal equation of state in a harmonic trap. We suggest improvements to our numerical methods which we expect to improve the quantitative agreement of the quadrupole mode frequency with the expected value outside of the hydrodynamic limit. We also suggest techniques for extracting the non-dominant (non-hydrodynamic) damping rate of the quadrupole mode in the hydrodynamic regime with higher precision. Additionally, we propose that the observed non-hydrodynamic damping of the quadrupole mode would be interesting to study experimentally for applications to collective oscillations in the quark-gluon plasma.

Acknowledgements

I first and foremost would like to thank Paul Romatschke for the incredible amount of guidance and support he has shown me in the course of the research presented in this thesis and for his primary role in inspiring me with my enthusiasm for research in theoretical physics. I would also like to thank several professors who have had a formative role in my undergraduate career - Mihalay Horanyi, to whom I owe the fact that I "found" physics as an unhappy engineering student; David Grant, to whom I largely owe my sense of wonderment and awe with regards to the beauty of the field of mathematics; and Eric Zimmerman, to whom I am indebted for his good advice and teaching. The content of this thesis owes a lot to the work of Miller Mendoza, who visited us for a week in the summer of 2014 from ETH Zürich to provide solutions to several problems in the implementation of the lattice Boltzmann method which had halted my progress. We corresponded with Marco Koschorreck, Tilman Enss, and Ana Maria Rey regarding the content of this thesis and acknowledge their time and support. Thanks to Will Lewis for being the only one of my peers brave enough to read this thesis thoroughly and provide thoughtful and relevant suggestions. This thesis contains several figures which were created for our paper [1], some of which were created by Paul Romatschke and some of which were created by me. I try to be particularly careful to cite our paper in cases where I use contributions that were made by other authors.

Contents

Chapter

Figures

Figure

Chapter 1

Introduction

Strong interactions in many-fermion systems lead to peculiar behaviors in materials important across high energy and condensed matter physics and astrophysics. The strongly-coupled quark gluon plasma created in heavy ion collisions exhibits elliptic flow instead of expanding isotropically [2]. Neutron stars exhibit neutron superfluidity and possibly quark superfluidity [3]. Certain materials (namely, the cuprates) exhibit transitions to superconducting states at critical temperatures orders much higher than can be explained by the celebrated Bardeen-Cooper-Schrieffer theory of superconductivity [4]. Among the simplest and most experimentally accessible strongly-coupled fermion system known currently are ultra-cold dilute gases of fermions. Fermi gases have emerged onto the forefront of physics in recent years as a prototypical system in which to study strong interactions in systems which are more difficult to study experimentally.

Fermi gases are ultra-cold dilute gases of fermionic atoms [5]. The interaction between atoms scales with the s-wave scattering length a and can be tuned in experiments to explore the dynamics of the gas as a function of the fermion-fermion interaction strength between weak attractive interactions (Bardeen-Cooper-Schreiffer pairing) and strongly attractive bound states (Bose-Einstein condensation). The unitary limit occurs at the interaction strength where bound states are just formed, and is characterized by the divergence of the scattering length $a \to \infty$. The unitary limit of the unitary Fermi gas is interesting because the divergence of the scattering length renders the system "universal" in the sense that it lacks a characteristic length scale.

The so-called unitary regime of the Fermi gas is the regime of strongest fermion-fermion

interactions. The hydrodynamic equations governing evolution of the Fermi gas in this regime are scale invariant and approximately invariant under conformal transformations [6]. This characteristic is important to one of the theoretical motivations for studying unitary Fermi gases. It has been proposed that dynamics in higher-dimensional gravity can be formally related to corresponding dynamics in a dual conformal field theory. Through this correspondence in string theory, Kovtun, Son, and Starinets [7] showed that the ratio of shear viscosity to entropy density has an absolute lower bound $\eta/s > \hbar/4\pi k_B$. Quark gluon plasma and the unitary Fermi gas have $\eta/s \lesssim \hbar/2k_B$ [8], and are therefore among the best candidates for saturating or exceeding this lower bound. There is much interest in understanding the temperature, density, and other dependences of shear viscosity in the unitary Fermi gases for the purpose of testing this conjecture.

Beyond seeking a lower bound on shear viscosity in the Fermi gas, the unitary regime has other interesting properties. The crossover regime from weak to strong coupling which can be observed in the Fermi gas is relevant to weak-strong coupling crossovers in other materials. As is pointed out in Ref. [5], there is broad interest in understanding the dependence of the equation of state and transport properties of a quantum fluid on the interaction strength in a crossover between weak and strong coupling. In the majority of interesting physical cases however, these questions cannot be answered by purely analytic means. In this thesis we present a versatile numerical scheme for studying hydrodynamics in the crossover regime of the Fermi gas which may be used to investigate these and other open problems in strongly-interacting cold atomic gases.

In the present work we have developed fully nonlinear dissipative hydrodynamics simulations in two and three dimensions which we test by comparison with analytic solutions. We then present a study of collective oscillations in two-dimensional Fermi gases with ideal equation of state in a perfectly harmonic trapping potential and non-ideal equation of state in a gaussian trapping potential. We conclude with a discussion of applications of this and similar simulations to studying problems in physics which were not covered in this work.

This document is organized as follows: First we will introduce continuum hydrodynamics from the perspective of kinetic theory and the Boltzmann equation. We then hope to motivate

the lattice Boltzmann framework, by which hydrodynamics in continuous space can be reproduced exactly from calculations on a finite set of points in position and velocity space. Finally we present a high-level overview of unitary Fermi gases and their experimental realization to motivate our numerical studies and show our results for the dependence on interaction strength of the frequency and damping rates of collective oscillation modes of the Fermi gas. We will conclude with a summary of results and discussion of future work.

Chapter 2

Hydrodynamics

In this chapter we will discuss the theories of continuum hydrodynamics and motivate the discretization scheme by which continuum hydrodynamics can be put on a lattice and solved on the computer. We henceforth adopt a system of units where $\hbar = k_B = 1$, and let latin indices i $\in \{1, ..., D\}$ where D is the number of spatial dimensions so that we can label spatial vectors $\mathbf{v}$ explicitly in terms of their components as v_i. We also use the notation $\partial_i \equiv \frac{\partial}{\partial x_i}$ for coordinates x_i.

2.1 Continuum Hydrodynamics

Hydrodynamics is a phenomenon in statistical mechanics which emerges from the complex, coupled microscopic dynamics of a macroscopic number of interacting particles. Although in principal the dynamics could be solved exactly by considering the coupled equations of motion for every particle in a fluid, the impracticality of doing this computation for any macroscopic system requires an alternative method. The typical approach is to consider a macroscopic fluid as a statistical ensemble whose bulk dynamics are described by the following macroscopic variables [9]:

the fluid mass density $\rho(\mathbf{x}, t) = m \cdot n(\mathbf{x}, t)$,

the macroscopic fluid velocity $\mathbf{u}(\mathbf{x}, t)$,

the (kinetic and internal) energy $\epsilon(\mathbf{x}, t)$,

the temperature $T(\mathbf{x}, t)$,

and the pressure $P(\mathbf{x}, t)$.

The pressure is related to the temperature and the density via the equation of state $P = P(n, T)$. An ideal gas has the simple equation of state $P = nT$, but in general this relation depends on specifics of the material and may be much more complicated.

2.1.1 The Boltzmann Equation

The Boltzmann transport equation (henceforth called the Boltzmann equation) was derived by Ludwig Boltzmann in 1872 to describe the macroscopic evolution of the hydrodynamic variables in terms of a particle distribution function $f = f(\mathbf{x}, \mathbf{v}, t)$ which describes the fractional distribution of particles in position and velocity space. f has the property that its integral over phase space $\int f(\mathbf{x}, \mathbf{v}, t) d^D\mathbf{x} d^D\mathbf{v}$ is the total number of particles $N(t)$. For an otherwise free system of interacting particles with phase space distribution f, the Boltzmann equation reads

$$\left[\partial_t + \mathbf{v} \cdot \nabla\right] f(\mathbf{x}, \mathbf{v}, t) = -C[f]. \tag{2.1}$$

The collision integral $C[f]$ depends on the specifics of the particle interactions, and the microscopic velocity $\mathbf{v}$ is the particular location in velocity space of a fluid element described by f. It will be important for the discussion that follows to distinguish the microscopic velocity $\mathbf{v}$ from the macroscopic, or average, velocity $\mathbf{u}$ of the fluid.

In the presence of an external potential the Boltzmann equation is modified to

$$\left[\partial_t + \mathbf{v} \cdot \nabla - \frac{\nabla U(\mathbf{x})}{m} \cdot \nabla_v\right] f(\mathbf{x}, \mathbf{v}, t) = -C[f], \tag{2.2}$$

where the operator ∇_v takes the gradient in velocity space

$$\nabla_v = \frac{\partial}{\partial v_x}\hat{x} + \frac{\partial}{\partial v_y}\hat{y} + \frac{\partial}{\partial v_z}\hat{z} \tag{2.3}$$

and $U(\mathbf{x})$ is the potential energy associated with a conservative force $\mathbf{F}(\mathbf{x}) = -\nabla U(\mathbf{x})$.

In general the collision integral $C[f]$ has complicated nonlinear dependence on the details of the microscopic interactions. However, for a fluid which has sufficiently strong interactions that it has a small non-equilibrium component, we can take the well-known Bhatnagar-Gross-Krook

(BGK) ansatz (see Ref. [10]) for the collision integral

$$C[f] = \frac{1}{\tau}(f - f_{\text{eq}}), \tag{2.4}$$

where τ is a characteristic relaxation time of the fluid that is associated with its shear viscosity η by

$$\tau = \eta/P, \tag{2.5}$$

where P is the pressure [11].

The collision integral $C[f]$ certainly must conserve the conserved fluxes of the hydrodynamic scheme (i.e mass, momentum, and energy for a second-order scheme). This is enforced if the equilibrium distribution f_{eq} is a static solution of the Boltzmann equation

$$\left(\mathbf{v}\cdot\nabla - \frac{\nabla U(\mathbf{x})}{m}\cdot\nabla_v\right) f_{\text{eq}} = 0. \tag{2.6}$$

The equilibrium solution then takes the form of a Maxwellian

$$f_{\text{eq}}(\mathbf{x},\mathbf{v},t) \propto e^{-\frac{(\mathbf{v}-\mathbf{u})^2}{2c_s^2(T)}}, \tag{2.7}$$

where $c_s(T) = \sqrt{\frac{T}{m}}$ is the speed of sound in the fluid at temperature T and $\mathbf{u} = \mathbf{u}(\mathbf{x},t)$ is the macroscopic fluid velocity.

In the Boltzmann formulation, the macroscopic hydrodynamic variables are identified as velocity moments of the particle distribution function

$$\rho \equiv m\int d^D\mathbf{v} f, \tag{2.8}$$

$$\rho\mathbf{u} \equiv m\int d^D\mathbf{v}\mathbf{v} f, \tag{2.9}$$

$$\epsilon \equiv \frac{m}{2}\int d^D\mathbf{v}\mathbf{v}^2 f \tag{2.10}$$

where ρ is the mass density, ϵ is the energy density, and D refers to the number of spatial dimensions. The constant of proportionality of the equilibrium distribution is determined by enforcing that the zeroth velocity moment in Eq. (2.8) is satisfied for the equilibrium distribution f_{eq}. Specifically, $\rho = m\int d^D\mathbf{v} f_{\text{eq}}$ implies

$$f_{\text{eq}}(\mathbf{x},\mathbf{v},t) = \frac{\rho}{mc_s^D(T)\sqrt{2^D\pi^D}} e^{-\frac{(\mathbf{v}-\mathbf{u})^2}{2c_s^2(T)}}. \tag{2.11}$$

The conservation of the second velocity moment Eq. (2.10) with the equilibrium distribution Eq. (2.34) then gives the total energy density ϵ to be the sum of kinetic and internal energy densities:

$$\epsilon = \frac{1}{2}\rho \mathbf{u}^2 + \frac{D}{2}\rho c_s^2(T). \tag{2.12}$$

The previous discussion outlined a kinetic theory approach to hydrodynamics in that we described the macroscopic hydrodynamic variables (ρ,$\mathbf{u}$, and ϵ) as emerging out of the local transport of an underlying microscopic distribution. To connect this discussion with the systems of partial differential equations which are more conventionally associated with hydrodynamics, we note that the Navier-Stokes equations are derived by enforcing that up to second-order velocity moments of the Boltzmann equation are satisfied. For example, the zeroth velocity moment of the free-space Boltzmann equation is

$$\int \left(\frac{\partial}{\partial t} + \mathbf{v} \cdot \nabla \right) f(\mathbf{x}, \mathbf{v}, t) d^D \mathbf{v} = - \int C[f] d^D \mathbf{v}. \tag{2.13}$$

Since we require that the collision integral $C[f]$ conserves mass, $\int C[f] d^D \mathbf{v} = 0$. Therefore we obtain the free-space continuity equation of the Navier-Stokes equations from evaluating Eq. (2.13) using the definitions of the macroscopic variables as velocity moments of f in Eqs. (2.8) and (2.9):

$$\frac{\partial \rho}{\partial t} + \nabla \cdot \rho \mathbf{u} = 0. \tag{2.14}$$

The momentum and energy conservation Navier-Stokes equations can be derived similarly from first and second velocity moments of the Boltzmann equation. From this perspective, it is clear that hydrodynamics doesn't "stop" at the Navier-Stokes level - in principle, arbitrarily high velocity moments of the Boltzmann equation are associated with some conserved flux. Hydrodynamics beyond the Navier-Stokes level is even qualitatively relevant to understanding dynamics in many fluid systems.

2.2 Discrete Hydrodynamics

There are several ways in which we could proceed to calculate the macroscopic hydrodynamic behavior in terms of the observables $\rho(\mathbf{x}, t)$, $\mathbf{u}(\mathbf{x}, t)$, $\epsilon(\mathbf{x}, t)$, etc. We could solve a system of partial differential equations describing the conservation of the hydrodynamic variables. We could calculate the macroscopic hydrodynamic variables explicitly from Eqs. (2.8), (2.9), and (2.10), either analytically or by numerical integration, assuming that the particle distribution function $f(\mathbf{x}, \mathbf{v}, t)$ is known. Alternatively, if $f(\mathbf{x}, \mathbf{v}, t)$ is known, it is reasonable to ask whether there is a way to compute the moments in Eqs. (2.8), (2.9), and (2.10) without evaluating any integrals. In the lattice Boltzmann framework, the integral moments in Eqs. (2.8), (2.9), and (2.10) become sums over a finite set of velocities.

2.2.1 The Lattice Boltzmann Framework

As mentioned above, the idea of the lattice Boltzmann framework is to reduce the integral velocity moments of the particle distribution function to sums of the particle distribution function over a finite set of cleverly-chosen velocities which exactly match the values of the integrals. Then the exact calculation of $\rho(\mathbf{x}_i, t)$, $\mathbf{u}(\mathbf{x}_i, t)$, etc. at a finite set of position coordinates $\mathbf{x}_i$ requires knowledge of the particle distribution function only at a finite set of coordinates in phase space $f(\mathbf{x}_i, \mathbf{v}_i, t)$. The lattice Boltzmann method concerns itself with tracking the particle distribution function $f(\mathbf{x}_i, \mathbf{v}_i, t_i)$ as it evolves in discretized time $t_{i+1} = t_i + \delta t$ and uses this information to calculate the macroscopic hydrodynamic variables in discretized time and space $\rho(\mathbf{x}_i, t_i)$, etc. In the following sections, we will discuss the derivation and use of this method to discretize hydrodynamics and solve it on the computer.

2.2.1.1 Discrete Evolution

We first motivate the discrete Boltzmann equation by noting that, for small δt, the Boltzmann equation can be approximated using the limit definition of the derivative df/dt. Specifically, we

have

$$\frac{df}{dt} = \frac{\partial f}{\partial t} + \frac{d\mathbf{x}}{dt}\frac{\partial f}{\partial \mathbf{x}} \approx \frac{f(\mathbf{x} + \frac{d\mathbf{x}}{dt}\delta t, t + \delta t) - f(\mathbf{x}, t)}{\delta t} \tag{2.15}$$

Noting that $\frac{d\mathbf{x}}{dt} = \mathbf{v}$ and $\frac{\partial f}{\partial \mathbf{x}} = \nabla f$, we have a discrete approximation to the Boltzmann equation

$$\left[\partial_t + \mathbf{v} \cdot \nabla\right] f \approx \frac{f(\mathbf{x} + \mathbf{v}\delta t, t + \delta t) - f(\mathbf{x}, t)}{\delta t}. \tag{2.16}$$

For the Boltzmann equation with an external force per unit mass $\mathbf{F} = -\frac{\nabla U(\mathbf{x})}{m}$, we have

$$\left[\partial_t + \mathbf{v} \cdot \nabla - \frac{\nabla U(\mathbf{x})}{m} \cdot \nabla_v\right] f \approx \frac{f(\mathbf{x} + \mathbf{v}\delta t, t + \delta t) - f(\mathbf{x}, t)}{\delta t} + \mathbf{F} \cdot \nabla_v f \tag{2.17}$$

We note however that 2.16 only recovers the Boltzmann equation up to first order in derivatives, since we have

$$f(\mathbf{x} + \mathbf{v}\delta t, t + \delta t) - f(\mathbf{x}, t) = \left[\partial_t + \mathbf{v} \cdot \nabla\right] \delta t f + \frac{1}{2}\left[\partial_t + \mathbf{v} \cdot \nabla\right]^2 \delta t^2 f + ... \tag{2.18}$$

Therefore to recover the continuum Boltzmann equation up to second order in derivatives in our discrete scheme requires that we introduce numerical corrections to some of the parameters in the Boltzmann equation to cancel unwanted terms.

To proceed with the numerical implementation, we formulate a dimensionless version of the Boltzmann equation by selecting a length scale $R_\perp$ and a frequency (inverse-time) scale $\omega_\perp$ by which to normalize space and time coordinates. For the moment we leave these values arbitrary, and will associate them with physical values later when it becomes clear how best to simplify the equations. We have non-dimensional coordinates

$$\mathbf{x} = \bar{\mathbf{x}} R_\perp \qquad \bar{t} = t\omega_\perp \tag{2.19}$$

which are hence associated with velocity re-scalings

$$\mathbf{v} = \bar{\mathbf{v}} R_\perp \omega_\perp \qquad \mathbf{u} = \bar{\mathbf{u}} R_\perp \omega_\perp. \tag{2.20}$$

The Boltzmann equation is given in terms of these dimensionless coordinates as

$$\left(\partial_{\bar{t}} + \bar{\mathbf{v}} \cdot \bar{\nabla} - \frac{1}{R_\perp^2 \omega_\perp^2 m} \bar{\nabla} U(\bar{\mathbf{x}}) \cdot \bar{\nabla}_v\right) = -\frac{f - f_{\text{eq}}}{\tau \omega_\perp}. \tag{2.21}$$

For convenience in simplifying this equation, we can choose our normalization length scale $R_\perp$ to be [1]

$$R_\perp = \sqrt{\frac{T_0}{mc_L^2\omega_\perp^2}} \tag{2.22}$$

so that 2.21 takes its final form

$$\left(\partial_{\bar{t}} + \bar{\mathbf{v}}\cdot\bar{\nabla} - \frac{c_L^2}{T_0}\bar{\nabla}U(\bar{\mathbf{x}})\cdot\bar{\nabla}_v\right) f = -\frac{f - f_{\text{eq}}}{\tau\omega_\perp}. \tag{2.23}$$

The associated dimensionless equilibrium distribution is

$$f_{\text{eq}}(\bar{\mathbf{x}}, \bar{\mathbf{v}}, \bar{t}) = \frac{\rho}{mc_s^3(T)\sqrt{8\pi^3}} e^{-\frac{(\bar{\mathbf{v}}-\bar{\mathbf{u}})^2}{2c_L^2\theta}}, \tag{2.24}$$

where $\theta = T/T_0$ is a dimensionless temperature coordinate.

To recover the Boltzmann equation up to second order in derivatives using the left-hand side of Eq. (2.18), we can now define numerical corrections that cancel the higher-order terms of Eq. (2.18) that do not appear in the Boltzmann equation [1]:

$$\begin{aligned}
\tilde{\mathbf{u}} &= \mathbf{u} - \frac{\delta t}{2}\mathbf{F}\,, \\
\tilde{\tau} &= \frac{1}{2} + \frac{\omega_\perp \tau}{\delta t}\,, \\
\tilde{\mathbf{F}} &= \mathbf{F}(1 - \frac{\delta t}{2\tau}).
\end{aligned} \tag{2.25}$$

where numerically-corrected variables are indicated with a tilde. The replacements $\mathbf{u} \to \tilde{\mathbf{u}}$, $\tau \to \tilde{\tau}$, and $\mathbf{F} \to \tilde{\mathbf{F}}$ in the dimensionless Boltzmann equation Eq. (2.21) allow the evolution scheme Eq. (2.17) to be exact up to second-order in derivatives.

2.2.1.2 Gauss-Hermite Quadrature

In one dimension, the Maxwellian distribution $e^{-(v-u)^2/2}$ is the generating function of the Hermite polynomials $H_n(v)$:

$$e^{-(v-u)^2/2} = e^{-v^2/2}\sum_{n=0}^{\infty} H_n(v)\frac{u^n}{n!}. \tag{2.26}$$

The particle distribution function can be cast in terms of the tensor Hermite polynomials $H_n^{i_1\cdots i_n}$ as (see Ref. [12])

$$f(\mathbf{x},\mathbf{v},t) = e^{-\mathbf{v}^2/2} \lim_{N\to\infty} \sum_{n=0}^{N} H_n^{i_1,\ldots,i_n}(\mathbf{v}) \frac{a_n^{i_1\ldots i_{2n}}}{n!} \tag{2.27}$$

The Gauss-Hermite quadrature gives that the integrals $\int e^{-v^2/2} P(\mathbf{v}) d\mathbf{v}$ can be calculated exactly as a sum over the roots of $H_n(\mathbf{v})$ if $P(\mathbf{v})$ is a polynomial having degree $d \leq 2N$.

Therefore there exists a set of weights w_i for which sums over the set of roots ξ_i of $H_n(\mathbf{v})$ exactly reproduce the integrals in Eqs. (2.8), (2.9), and (2.10):

$$\begin{aligned} \textstyle\sum_i w_i f_i &= m \textstyle\int d^D\mathbf{v} f \,, \\ \textstyle\sum_i w_i \xi_i f_i &= m \textstyle\int \; d^D\mathbf{v}\mathbf{v} f \,, \\ \textstyle\sum_i w_i \xi_i^2 f_i &= m \textstyle\int d^D\mathbf{v}\mathbf{v}^2 f. \end{aligned} \tag{2.28}$$

We note that the set of ξ_i represents a discrete sampling in velocity space. If N is large enough, it possible to exactly calculate the macroscopic hydrodynamic variables up to arbitrary order in velocity moments, i.e.

$$\sum_i w_i \xi_i^M f_i = m \int d^D\mathbf{v}^M f. \tag{2.29}$$

This forms the basis of the lattice Boltzmann method. If we further discretize the spatial coordinates, we obtain lattices of discrete points in position space which are connected to one another by the velocities ξ_i. The set ξ_i describes every velocity by which a particle can move from one point in position space to another in one time step δt. Fig. 2.1 shows a basic phase space discretization scheme for the lattice Boltzmann method in two and three dimensions. The center is a specific location in position space, and the vectors indicate the possible velocities of a particle at that point.

The idea of computing the discrete versions of the equilibrium distribution f_{eq} and the forcing term is that we enforce that the sums and integrals match exactly up to the hydrodynamic order which we wish to recover. It is important to notice that although it is possible to match arbitrarily high velocity moments of the particle distribution function in this way, successively higher velocity moments can only be computed on successively higher-order lattices. The lattice which we use in

Figure 2.1: Standard D2Q9 (2 dimensions and 9 speeds) and its three-dimensional extension D3Q19 (3 dimensions and 19 speeds).

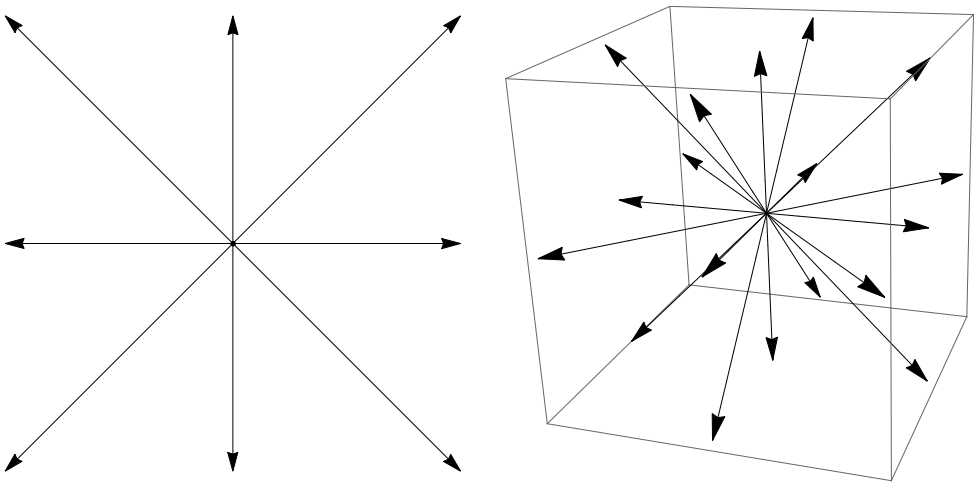

this work is less common than the two-dimensional lattice pictured in Fig. 2.1 and recovers higher order velocity moments than is possible with that lattice. We use a lattice with 2 dimensions and 25 velocities (called D2Q25) pictured in Fig. 2.2.

Lattices are required to have a set of discrete symmetries to represent physical symmetries in the physical system. For example, we enforce that quantities we associate with probabilities sum to one, and that our lattice has discrete rotational symmetry. The lower order symmetries are shown in Eq. (2.30). See Ref. [9] for discussion of higher order lattice symmetries.

$$\begin{aligned} \textstyle\sum_i w_i &= 1\,, \\ \textstyle\sum_i w_i \xi_i &= 0\,, \\ \textstyle\sum_i w_i \xi_i \xi_i &= c_L^2 \mathbf{I}. \end{aligned} \tag{2.30}$$

Here $\mathbf{I}$ is the identity. It is important to note that the final relation in Eq. (2.30) and Eq. (2.12) together limit the fluid velocity $\mathbf{u}$ in any direction in dimensionless units to be less than c_L. The existence of a maximal velocity on the lattice is intuitive because each of the discretization schemes shown in Figs. 2.1 and 2.2 have maximum distances that a particle can "hop" on a time step. Since the D2Q25 lattice shown in Fig. 2.2 has longer possible velocities than the D2Q9 lattice shown in Fig. 2.1, its lattice velocity c_L is also larger. The value of c_L for a specific discretization scheme can be computed from Eq. (2.30), and in particular $c_L^2 = 1 - \sqrt{2/5}$ for D2Q25 and $c_L^2 = 1/3$ for D2Q9. Therefore, in addition to recovering higher-order velocity moments of the distribution function, the D2Q25 lattice has the advantage of supporting fluids which obtain higher velocities.

Figure 2.2: The extended two-dimensional lattice with 25 velocities which is used for the simulations proposed in this thesis

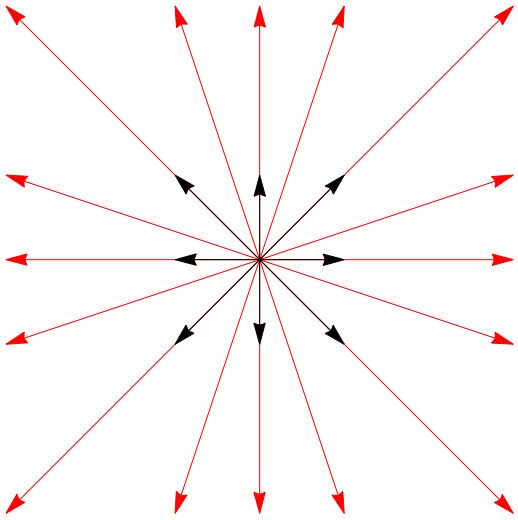

2.2.1.3 Equilibrium Distribution

The Hermite polynomials form an orthogonal basis set for the equilibrium distribution. In index notation, the relevant tensor Hermite polynomials are

$$\begin{aligned} P_0(v) &= 1\,, \\ P_1^i(v) &= v^i\,, \\ P_2^{ij}(v) &= v^i v^j - c_L^2 \delta^{ij}\,, \\ P_2^0(v) &= Tr(P^{ij}(v)) = v^2 - Dc_L^2. \end{aligned} \tag{2.31}$$

where D is the number of dimensions and c_L is the lattice speed of sound, the maximum speed which can be supported by the geometry of a particular lattice. Then we have from the Gauss-Hermite quadrature that

$$e^{-\frac{(\mathbf{v}-\mathbf{u})^2}{2c_L^2\theta}} = e^{-\frac{\mathbf{v}^2}{2c_L^2}} \left(a_0 P_0 + a_i P_1^i + a_{ij} P_2^{ij} + a_2^0 P_2^0 + ...\right), \tag{2.32}$$

where a sum over spatial dimensions of like indices is implied, e.g. $a_{ij}P^{ij} = \sum_i \sum_j a_{ij}P^{ij}$ where i, j index the components of the tensors a and P. The coefficients a_0, a_i, a_{ij} and a_2^0 are calculated by enforcing that the following equations are satisfied:

$$\begin{aligned} \sum w_k \left(a_0 P_0 + a_i P_1^i + a_{ij} P_2^{ij} + a_2^0 P_2^0\right) &= \int d^D\mathbf{v} f_{\text{eq}}\,, \\ \sum w_k \mathbf{v} \left(a_0 P_0 + a_i P_1^i + a_{ij} P_2^{ij} + a_2^0 P_2^0\right) &= \int d^D\mathbf{v}\mathbf{v} f_{\text{eq}}\,, \\ \sum w_k \left(\mathbf{v}^2 - Dc_L^2\right) \left(a_0 P_0 + a_i P_1^i + a_{ij} P_2^{ij} + a_2^0 P_2^0\right) &= \int d^D \left(\mathbf{v}^2 - Dc_L^2\right) f_{\text{eq}}. \end{aligned} \tag{2.33}$$

Including up to third order polynomials gives the equilibrium distribution [1]

$$\begin{aligned} f_{\text{eq}} = \frac{n}{\sqrt{2^D \pi^D} c_s^3(T_0)} e^{-\frac{\bar{\mathbf{v}}^2}{2c_L^2}} \quad & \left[1 + \frac{\bar{\mathbf{u}}\cdot\bar{\mathbf{v}}}{c_L^2}\left(1 + \frac{\theta-1}{2c_L^2}(\bar{\mathbf{v}}^2 - (D+2)c_L^2)\right) + \frac{(\bar{\mathbf{u}}\cdot\bar{\mathbf{v}})^2}{2c_L^4} - \frac{\bar{\mathbf{u}}^2}{2c_L^2}\right. \\ & \left. + \frac{\theta-1}{2c_L^2}\left(\bar{\mathbf{v}}^2 - Dc_L^2\right) + \frac{(\bar{\mathbf{u}}\cdot\bar{\mathbf{v}})^3}{6c_L^6} - \frac{\bar{\mathbf{u}}^2(\bar{\mathbf{u}}\cdot\bar{\mathbf{v}})}{2c_L^4}\right]. \end{aligned} \tag{2.34}$$

The temperature parameter is $\theta = T/T_0$ for an ideal equation of state $P = nT$. For non-ideal equations of state $P = P(n, T)$, we have $\theta = \frac{P}{nT_0}$.

2.2.1.4 Discretization of External Force

The term in the Boltzmann equation associated with an external force

$$-\frac{c_L^2}{T_0}\bar{\nabla}U(\bar{\mathbf{x}})\cdot\bar{\nabla}_v f \tag{2.35}$$

can be similarly discretized in terms of the Hermite polynomials as

$$\frac{c_L^2}{T_0}\bar{\nabla}U(\bar{\mathbf{x}})\cdot\bar{\nabla}_v f = e^{-\frac{\bar{\mathbf{v}}^2}{2c_L^2}}\left(a_0P_0 + a_iP_1^i + a_{ij}P_2^{ij} + a_2^0P_2^0 + ...\right). \tag{2.36}$$

Defining the dimensionless force $\bar{\mathbf{F}} = -\frac{c_L^2}{T_0}\bar{\nabla}U(\bar{\mathbf{x}})$, we have [1]

$$\begin{aligned}\bar{\mathbf{F}}\cdot\nabla_v f = \frac{n}{\sqrt{2^D\pi^D}c_s^3(T_0)}\frac{e^{-\frac{\bar{\mathbf{v}}^2}{2c_L^2}}}{c_L^2}\Bigg[-\bar{\mathbf{u}}\cdot\bar{\mathbf{F}}\left(1+\frac{\bar{\mathbf{u}}\cdot\bar{\mathbf{v}}}{c_L^2}\right)+\bar{\mathbf{v}}\cdot\bar{\mathbf{F}}\\ \left(1+\frac{\bar{\mathbf{v}}\cdot\bar{\mathbf{u}}}{c_L^2}+\frac{(\bar{\mathbf{v}}\cdot\bar{\mathbf{u}})^2}{2c_L^4}-\frac{\bar{\mathbf{u}}^2}{2c_L^2}+\frac{\theta-1}{2}\left(\frac{\bar{\mathbf{v}}^2}{c_L^2}-(D+2)\right)\right)\Bigg]\end{aligned} \tag{2.37}$$

2.2.1.5 The Algorithm

We finally conclude by presenting the procedure for calculating the macroscopic hydrodynamic variables $\rho(\mathbf{x},t)$, $\mathbf{u}(\mathbf{x},t)$, and $\epsilon(\mathbf{x},t)$ using the ingredients prescribed above.

The lattice Boltzmann algorithm prescribes the evolution of the particle distribution function $f(\mathbf{x}_i,\mathbf{v}_i,t_i)$ on a lattice of points $\mathbf{x}_i$ in space, and at discrete time intervals t_i. The evolution is given by the following procedure:

1). Prescribe the initial state of the particle distribution function by specifying the initial state macroscopic variables $\rho(\mathbf{x}_i,0)$, $\mathbf{u}_i(\mathbf{x}_i,0)$, and $\epsilon(\mathbf{x}_i,0)$ and assuming that the fluid is in equilibrium $f(\mathbf{x}_i,\mathbf{v}_i,0) = f_{\rm eq}(\rho(\mathbf{x}_i,0),\mathbf{u}(\mathbf{x_i},0),\epsilon(\mathbf{x}_i,0))$.

2). Calculate the (numerically-corrected) macroscopic variables ρ, $\tilde{\mathbf{u}}$ and ϵ as the sums in Eq. (2.28) with the numerical corrections given in Eq. (2.25).

3). Use the newly-calculated values of the macroscopic variables (and $\mathbf{u}\leftarrow\tilde{\mathbf{u}}$) to calculate the discretized versions of the equilibrium distribution $f_{\rm eq}$ and the force term $\bar{\mathbf{F}}\cdot\nabla_v$.

4). Temporarily replace $f(\mathbf{x}_i, \mathbf{v}_i, t)$ by its equilibrium-relaxed value

$$f(\mathbf{x}_i, \mathbf{v}_i, t) = f(\mathbf{x}_i, \mathbf{v}_i, t)\left(1 - \frac{1}{\tau}\right) + f_{\text{eq}}(\mathbf{x}_i, \mathbf{v}_i, t)\frac{1}{\tau} + \bar{\bar{F}} \cdot \nabla_v f(\mathbf{x}_i, \mathbf{v}_i, t) \tag{2.38}$$

5). Propagate the particle distribution function according to the evolution equation Eq. (2.17) to advance to the next time step $t_{i+1} = t_i + \delta t$.

6). Repeat the procedure from step 2 for each successive time step.

Chapter 3

Unitary Fermi Gases

3.1 Background

Ultracold dilute gases of fermions, called Fermi gases, have emerged onto the forefront of physics in recent years due to the experimental realization of Bose-Einstein condensation (BEC) in a dilute gas of bosons in 1995 [13] and of degenerate Fermi gases in 1999 [14]. The unitary regime of the Fermi gas is in the crossover regime between Bose-Einstein condensation and Bardeen-Cooper-Schriefer (BCS) states [15]. BEC is a regime in which fermions form two-body bound states, rendering them composite bosons. BCS is a regime in which fermions pair weakly across the Fermi surface (see Fig. 3.1). In the crossover regime between these pairing structures is the most strongly-interacting state [16].

Figure 3.1: This cartoon depicts fermion pairing as a function of interaction energy for the BEC-BCS crossover. Reproduced from [16].

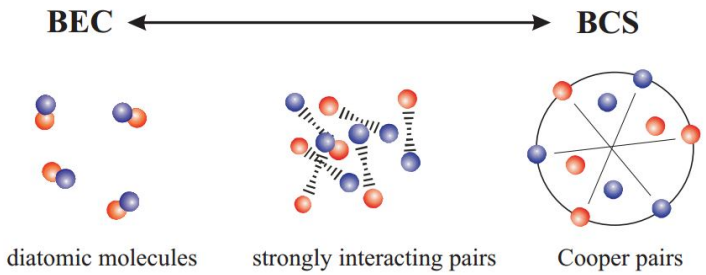

In cold atomic gas experiments, collections of atoms (often Potassium) are cooled to tem-

peratures on the order of milli-Kelvins and loaded into optical traps which spatially confine the atoms. Optical lattices enable the study of two-dimensional atomic gases because strong confinement in one direction "freezes out" the degrees of freedom in that direction and makes the system effectively two-dimensional. For the two-dimensional Fermi gas experiments we consider in this thesis, there are several traps which each confine a two-dimensional gas with an isotropic Gaussian density profile, somewhat like a stack of pancakes. The probability of quantum tunneling between the individual two-dimensional gases should be negligible for our numerical solutions (which do not account for this effect) to remain accurate.

Fermi gases are simpler to study than many other strongly-coupled fermion systems because the fermion-fermion interaction strength can be tuned in experiment using a variable attractive potential. In particular, the van der Waals interaction is an attractive potential between two atoms which is due to interactions between both permanent and induced dipoles and can be tuned via a homogenous magnetic field. The attractive potential is very sensitive to the magnetic field near a scattering Feshbach resonance. This characteristic can be used to tune fermion-fermion interactions in a Fermi gas through the BCS-BEC crossover regime.

We study in this thesis gases which are in the normal phase, meaning that they are at a temperature above the superfluid phase transition temperature T_c. In principal the hydrodynamic description is also applicable to the study of superfluids, however the approach is typically to use two-fluid hydrodynamics to describe separately the normal and superfluid components of the fluid.

3.2 Hydrodynamics in cold atomic gases

Hydrodynamics is a valid theory for near-equilibrium statistical ensembles, and is therefore relevant when dynamics occur on long time scales relative to the characteristic equilibration time τ of the system. This is certainly satisfied for all dynamics in the so-called hydrodynamic limit $\tau \to 0$. Since τ is proportional to the shear viscosity η as in Eq. (2.5), the hydrodynamic limit also corresponds to $\eta \to 0$, and consequently the divergence of the scattering length $a \to \infty$. Therefore the hydrodynamic limit of the Fermi gas is precisely the unitary regime. Hydrodynamics is also

quantitatively applicable outside of the limit $\tau \to 0$, so we expect hydrodynamics to work in general near the unitary regime where a is large.

Furthermore, it is not necessarily immediately clear that we can validly assume classical Boltzmann statistics for a fluid which should clearly exhibit quantum statistics. In [1], we note that accurately representing the macroscopic hydrodynamic variables does not indicate that we have accurately represented the underlying particle distribution. We do not claim to accurately represent the particle distribution function, and instead approach the use of hydrodynamics as an effective macroscopic theory.

Strongly interacting fluids have anomalously low viscosity, and are therefore candidates for "perfect fluids", which would saturate the lower bound $\eta/s = 1/4\pi$. To gain a qualitative understanding of the relationship between shear viscosity and interaction strength, we can approximate the shear viscosity in a fluid as [17].

$$\eta = \frac{\langle p \rangle}{3\sigma}, \tag{3.1}$$

where $\langle p \rangle$ is the mean momentum and σ is the collision cross-section for particles in the fluid. The collision cross-section increases with interaction strength, so Eq. (3.1) indicates that stronger fluid interactions will result in lower shear viscosity.

Chapter 4

Collective Oscillations in Unitary Fermi Gases

4.1 Background

A strongly-interacting fluid which experiences a perturbation from a stable solution exhibits macroscopic oscillations around equilibrium that are qualitatively different from those that would be observed in an ordinary weakly-interacting fluid. In two dimensions, any oscillation about a stationary center of mass is a linear combination of the breathing and quadrupole oscillatory modes depicted in Fig. 4.1.

Figure 4.1: Cartoons depicting breathing (left) and quadrupole (right) oscillatory modes. Reproduced from [18].

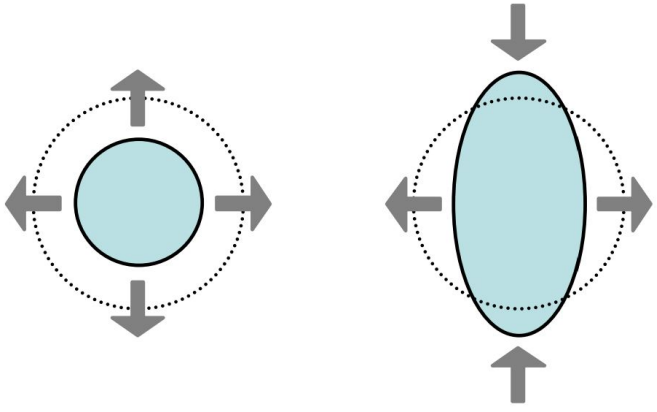

Collective oscillations in two-dimensional Fermi gases have been studied by the group of

Michael Köhl. In Ref. [19], they study the dependence of the frequency and damping of the breathing and quadrupole modes on the interaction strength $\ln(k_F a)$ near the unitary regime, where the Fermi momentum k_F is a normalization coefficient for the scattering length that depends on the number density [15]. Their results are reproduced in Fig. 4.2. Note that the two-dimensional scattering length a_{2D} in the figure is what we refer to as a. Although we do not present a quantitative analysis in this work relating $\ln(k_F a)$ to our $\omega_\perp \tau$, this is fairly straightforward and will be discussed in Ref. [1].

In the remainder of this chapter we present numerical studies of collective oscillations in two-dimensional Fermi gases. We first present our results for the case of a gas with ideal equation of state $P = nT$ in a harmonic trap, and compare to scaling solutions which we derive in this. Finally we present results for the case of a gas with non-ideal equation of state given by Ref. [20] in a Gaussian trap.

4.2 Thermal Model for Collective Oscillations

The temperature enters the model through the parameter θ in the equilibrium distribution Eq. (2.34). It has been shown Ref. [21] that a spatially- and time-dependent temperature can be included in the lattice Boltzmann method by inclusion of an internal energy distribution function $\epsilon(\mathbf{x}, \mathbf{v}, t)$ that obeys the same evolution equation as the particle distribution function but with a different characteristic relaxation time τ_E:

$$\epsilon(\mathbf{x} + \mathbf{v}\delta t, t + \delta t) - \epsilon(\mathbf{x}, t) = -\frac{1}{\tau_E}(\epsilon - \epsilon_{eq}). \tag{4.1}$$

However, we found in this study that the numerical stability of this thermal model was poor compared to that of the isothermal model and was sensitive to the boundary conditions placed on the internal energy distribution function. Therefore we opted to take the gas to have a temperature that is constant in space but is allowed to fluctuate in time. Specifically, we calculate θ at each time step to be

$$\theta = \frac{P}{2Nc_L^2}, \tag{4.2}$$

Figure 4.2: Data from two-dimensional Fermi gas experiments showing the dependence of oscillations frequency and damping rates on the interaction strength $\ln(k_F a)$ for breathing and quadrupole modes. ω_B and ω_Q are the frequencies of the breathing and quadrupole mode respectively; Γ_B and Γ_Q are the associated damping rates. The normalizations are relative to $\omega_\perp = \sqrt{\omega_x \omega_y}$ and ω_y, and an anisotropy of less than 2% implies that $\omega_y \approx \omega_y$. Reproduced from [19].

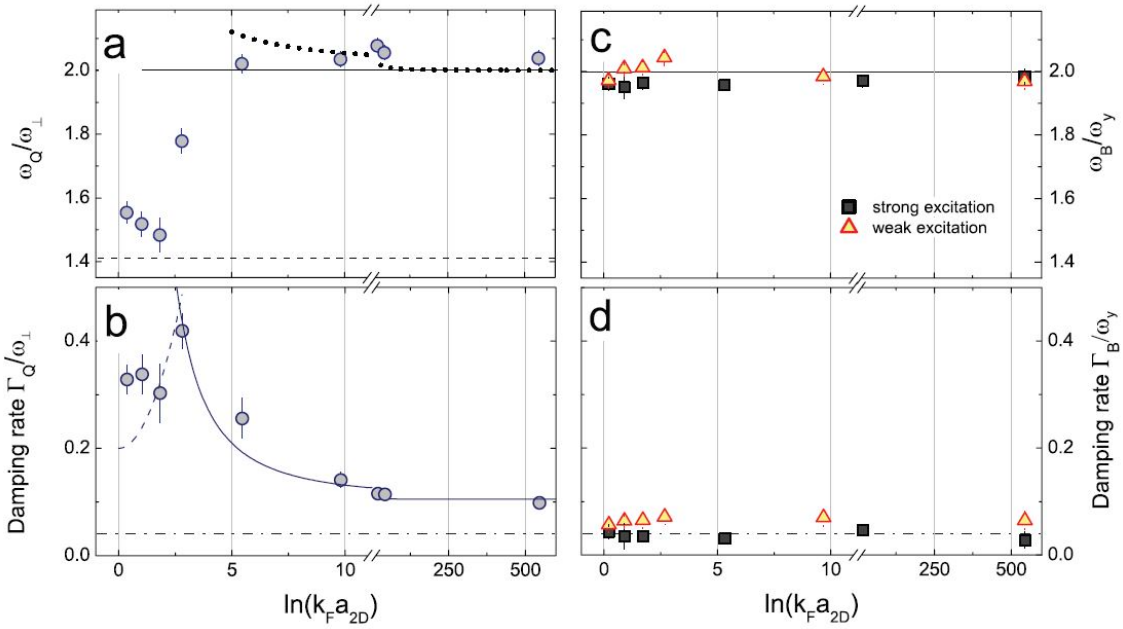

where P is the internal (potential) energy $P = \sum_{\mathbf{x}} \left(\epsilon(\mathbf{x}) - \rho(\mathbf{x})U(\mathbf{x})^2\right)$ and $N = \sum_{\mathbf{x}} \rho(\mathbf{x})$. ($\rho$, $\mathbf{U}$, and ϵ are velocity moments of the distribution function given in Eq. (2.28)).

4.3 Harmonic Traps

We first study the case of a strongly-interacting fluid with an ideal gas equation of state $P(n,T) = nT$ in a harmonic trap. Let σ denote the equilibrium standard deviation of an isotropic harmonic trapping potential and σ_x, σ_y be standard deviations in the $\hat{x}$ and $\hat{y}$ directions, so that in the equilibrium state $\sigma = \sigma_x = \sigma_y$. Then we excite a pure breathing mode oscillation by initializing our cloud with a symmetric non-equilibrium density profile $\sigma_x = \sigma_y \neq \sigma$. To excite the pure quadrupole mode, we initialize a cloud with an elongated density profile $\sigma_x \neq \sigma$ and $\sigma_y = 1/\sigma_x$. For the data shown in the following section, we excite both modes simultaneously by a deformation $\sigma_x = \sigma$ and $\sigma_y \neq \sigma$ and then separate the resulting oscillation into breathing and quadrupole mode components by $B(t) = \sigma_x(t) + \sigma_y(t)$ and $Q(t) = \sigma_x(t) - \sigma_y(t)$.

Fig. 4.3 shows the resulting time evolution of two-dimensional snapshots of the density profile for breathing mode and quadrupole mode oscillations.

4.3.1 Analytic Approach

In this case the force term in the Boltzmann equation is associated with a harmonic potential $U(\mathbf{x}) = \frac{1}{2}m\mathbf{x}^2$: $\mathbf{F} = -m\mathbf{x}$. In the following we derive scaling solutions for the breathing and quadrupole mode oscillations. This analysis follows closely a section in [1] written by P. Romatschke.

An equilibrium solution to the dimensionless Boltzmann equation

$$\left[\partial_{\bar{t}} + \bar{\mathbf{v}} \cdot \nabla - \frac{c_L^2}{T_0}\nabla U(\mathbf{x}) \cdot \nabla_v\right] f = -\frac{f - f_{\text{eq}}}{\tau\omega_\perp} \tag{4.3}$$

with $T = T_0$ and the ideal gas equation of state $P = nT$ is

$$f_0(\bar{\mathbf{x}}, \bar{\mathbf{v}}) = \frac{1}{\sqrt{8\pi^3}c_s^3(T_0)} e^{-\frac{\bar{\mathbf{v}}^2}{2c_L^2} - \frac{U(\bar{\mathbf{x}})}{T_0}}. \tag{4.4}$$

Figure 4.3: Two-dimensional simulated density profiles for quadrupole and breathing mode oscillations of unitary Fermi gases in a harmonic trap.

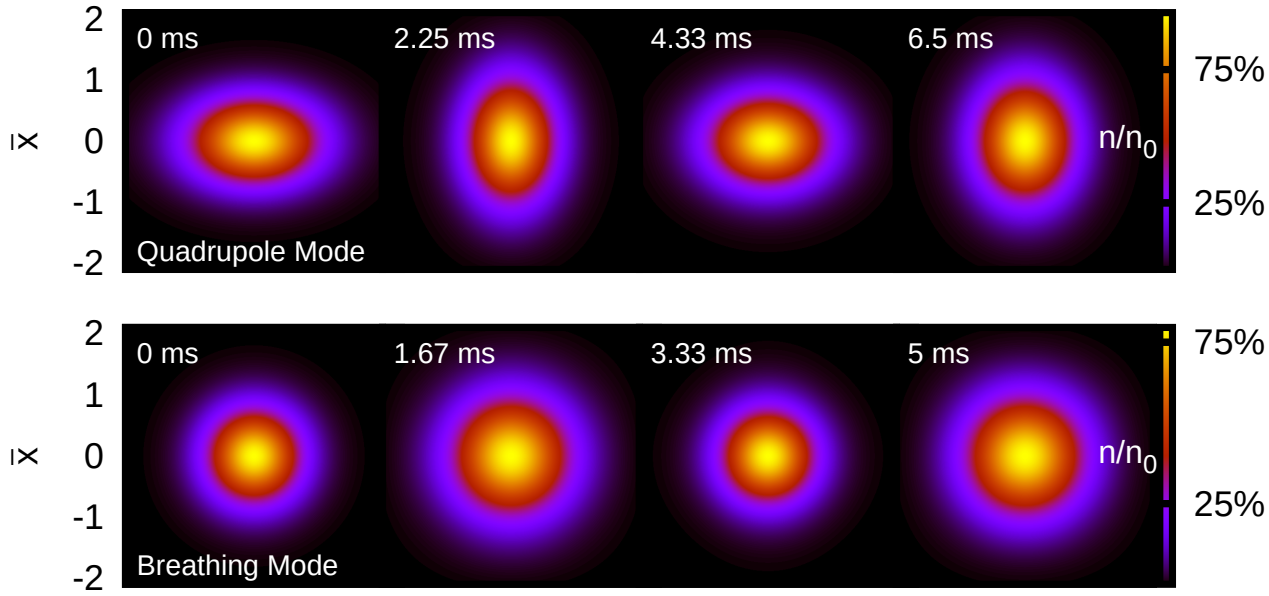

Ref. [11] takes the ansatz

$$f(\bar{\mathbf{x}}, \bar{\mathbf{v}}, \bar{t}) = f_0 \left(\frac{x_i}{b_i(\bar{t})}, \frac{b_i - x_i \dot{b_i}(t)/b_i(t)}{\theta_i^{1/2}(t)} \right) \tag{4.5}$$

for the particle distribution function and shows that integrals of the Boltzmann equation with this ansatz give a set of differential equations in scale parameters b_i and θ_i:

$$\ddot{b_i}(\bar{t}) + b_i(\bar{t}) - \frac{\theta_i(\bar{t})}{b_i(\bar{t})} = 0 \tag{4.6}$$

$$\dot{\theta_i}(\bar{t}) + 2\frac{\dot{b_i}(\bar{t})}{b_i(\bar{t})}\theta_i(\bar{t}) = -\frac{\theta_i(\bar{t}) - \bar{\theta}}{\tau\omega_\perp}. \tag{4.7}$$

Here $\bar{\theta}$ is the average value of the θ_i. Furthermore we associate the scale parameters b_i with the cloud width in the $\hat{i}$ direction and the θ_i's with a temperature coordinate. For small perturbations $b_i(\bar{t}) = 1 + \delta b_i(\bar{t})$, the equations decouple into a breathing mode $\delta B(\bar{t}) = \frac{1}{2}\left(\delta b_x(\bar{t}) + \delta b_y(\bar{t})\right)$ and a quadrupole mode $\delta Q(\bar{t}) = \frac{1}{2}\left(\delta b_x(\bar{t}) - \delta b_y(\bar{t})\right)$. With the initial conditions $b_i(0) = 1$ and $\delta\dot{b}_i(0) = 0$, Eqs. (4.6) and (4.7) become

$$\delta\ddot{B}(\bar{t}) + 4\delta B(\bar{t}) = 0. \tag{4.8}$$

$$\delta\ddot{Q}(\bar{t}) + 2\delta Q(\bar{t}) + \tau\omega_\perp \left(\delta\dddot{Q}(\bar{t}) + 4\delta\dot{Q}(\bar{t}) \right) = 0. \tag{4.9}$$

The solutions to these equations are an undamped breathing mode oscillation

$$\delta B(\bar{t}) = Ae^{-\Gamma_B \bar{t}} \cos(\omega_B \bar{t} + phase) \tag{4.10}$$

with $\Gamma_B = 0$ and a quadrupole mode oscillation

$$\delta Q(\bar{t}) = Be^{-\Gamma_0 \bar{t}} \cos(\omega_Q \bar{t} + phase) + Ce^{-\Gamma_1 \bar{t}}. \tag{4.11}$$

The term $Be^{-\Gamma_0 \bar{t}}$ dominates in the hydrodynamic limit $\tau \to 0$ and is therefore referred to as the hydrodynamic component of the quadrupole mode oscillation. The purely damped term $Ce^{-\Gamma_1 \bar{t}}$ is referred to as the non-hydrodynamic mode and arises only away from the hydrodynamic regime.

4.3.2 Numerical Results

Motivated by the scaling solutions Eqs. (4.10) and (4.11), we extract the frequencies and damping rates of $B(t) = b_x(t)+b_y(t)$ by a five-parameter nonlinear fit of the form $Ae^{-\Gamma_B \bar{t}}\cos(\omega_B \bar{t}+\phi_B)+\Delta_B$ and of $Q(t) = b_x(t)-b_y(t)$ by a seven-parameter nonlinear fit of the form $Be^{-\Gamma_0 \bar{t}}\cos(\omega_Q \bar{t}+\phi_Q) + Ce^{-\Gamma_1 \bar{t}} + \Delta_Q$. In Fig. 4.4 we show our numerical results for the frequencies and damping rates as a function of the normalized relaxation time τ compared to the scaling solutions Eq. (4.8).

Figure 4.4: Frequencies and damping rates of the breathing and quadrupole mode oscillations as a function of the dimensionless relaxation time $\omega_\perp \tau$ for a gas with ideal equation of state in a harmonic trap. Lines show the scaling solutions in Eq. (4.8) and dots are numerical results.

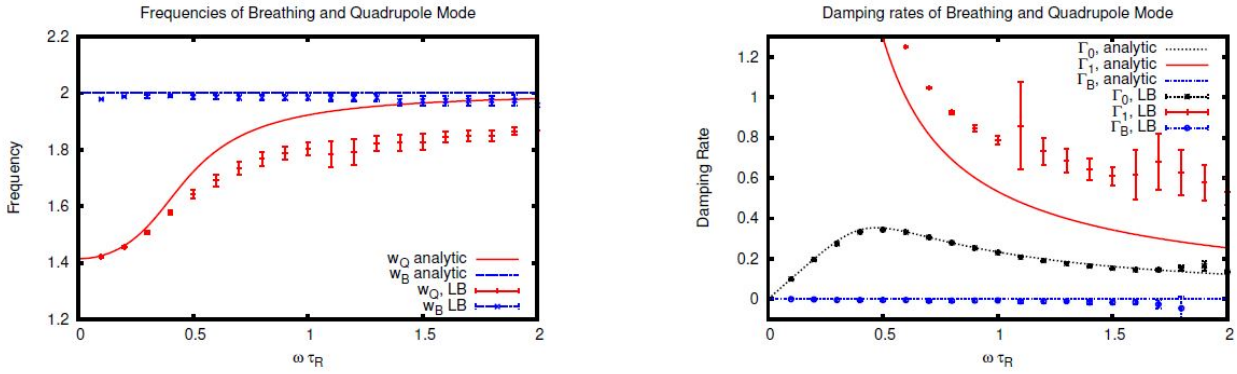

4.4 Gaussian Traps

It is extremely difficult to optically confine atoms in a purely harmonic trap because the Gaussian intensity distribution of a laser beam produces anharmonicities in the trapping potential [18]. Because scaling solutions are available only in the case of a harmonic trapping potential, we use our simulations to study unitary Fermi gases in Gaussian traps. A Gaussian potential is given by

$$U(\bar{\mathbf{x}}) = V_0(1 - e^{-\frac{\bar{\mathbf{x}}^2}{\sigma^2}}), \tag{4.12}$$

where V_0 is the potential depth. We calculate σ by enforcing that this Gaussian potential approximates our harmonic potential near the center of the trap $\bar{\mathbf{x}} = 0$. Since

$$V_0(1 - e^{-\frac{\bar{\mathbf{x}}^2}{\sigma^2}}) \approx V_0 \frac{\bar{\mathbf{x}}^2}{\sigma^2} \tag{4.13}$$

near $\bar{\mathbf{x}} = 0$ and the harmonic trapping potential associated with the dimensionless Boltzmann equation 2.21 is $U(\bar{\mathbf{x}}) = \frac{T_0 \bar{\mathbf{x}}^2}{2c_L^2}$, we associate $\sigma^2 = 2c_L^2 \frac{V_0}{T_0}$.

4.5 Non-Ideal Equation of State

Thus far in this analysis we have used the assumption that the unitary Fermi gas has the equation of state of an ideal gas. Enss et al. [20] suggest that in fact the equation of state of the Fermi gas even at moderate interaction strength is significantly different than the ideal prediction. The frequencies and damping rates of the collective mode oscillations in unitary Fermi gases are a good probe of the equation of state because the breathing mode frequency and damping rate is supposed to be sensitive to the equation of state, while the frequency of the quadrupole mode is not [18].

Enss et al. [20] computed the equation of state at finite temperature in the crossover regime using a self-consistent T-matrix approach (see [20]). We use this equation of state to calculate $\theta = \frac{P(n,T)}{nT_0}$ in the equilibrium distribution f_{eq}.

We test the non-ideal equation of state in harmonic and Gaussian traps. Fig. 4.5 shows the dependence of the mode frequencies and damping rates for a gas with this non-ideal equation of state in a Gaussian trap with $V_0/T_0 = 10$.

We note that the frequencies and damping rates of the gas with non-ideal equation of state in a Gaussian trap are qualitatively similar to those with an ideal equation of state in a harmonic trap. For gases with a non-ideal equation of state in a Gaussian trap however, the "undamped" breathing mode oscillation shows a low but distinctly non-zero damping rate. We also note that the frequencies of both the breathing and quadrupole modes are lower in the hydrodynamic limit $\tau \to 0$ for a gas with non-ideal equation of state in a Gaussian trap that for its harmonic and ideal

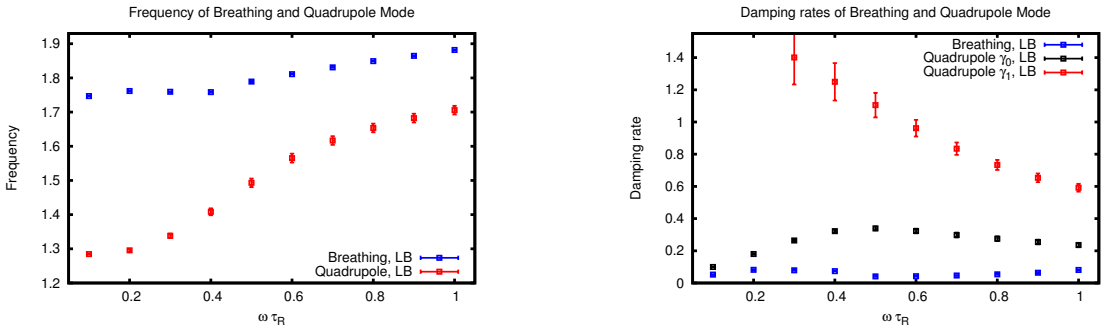

Figure 4.5: Frequencies and damping rates of the breathing and quadrupole mode oscillations as a function of the normalized relaxation time $\omega_\perp \tau$

counterparts.

Chapter 5

Conclusions and Future Work

We conclude by noting that we have produced two- and three-dimensional fully nonlinear lattice hydrodynamics simulations which can be used to study dynamics in unitary cold atomic gases. We have compared our numerical solutions to available analytic solutions in the case of collective oscillations of an ideal unitary Fermi gas in a perfectly harmonic trapping potential to study their accuracy. We see very good quantitative agreement between the breathing mode frequency and damping rate ω_B and Γ_B and the hydrodynamic quadrupole mode damping rate Γ_0 with the analytic solutions for all values of τ. We also see quantitative agreement with analytic solutions of the quadrupole mode frequency ω_Q in the hydrodynamic limit $\tau \to 0$. We see qualitative agreement also between the quadrupole mode frequency ω_Q and the non-hydrodynamic quadrupole mode damping rate Γ_1 for all values of τ. We propose in Ref. [1] that the disagreement of the quadrupole mode frequency outside of the hydrodynamic limit may be due to the fact that formally the lattice Boltzmann method only recovers continuum hydrodynamics in the hydrodynamic limit $\tau \to 0$. We expect that if this is the case, then using a finer velocity discretization scheme (e.g. a lattice with more possible velocities) will improve the agreement of our simulated quadrupole mode frequency ω_Q in a harmonic trap with the analytic results. We will test this in our future work.

The quantitative disagreement of the non-hydrodynamic mode damping Γ_1 with analytic results we attribute in Ref. [1] to the smallness of the term $e^{-\Gamma_1 \bar{t}}$ compared to $e^{-\Gamma_0 \bar{t}}$ which makes it uncertain to extract the value of Γ_1. For the same reason, we expect this parameter also to be difficult to determine with precision in experiments, though we suggest that it would be an

interesting parameter for experimentalists to record for applications of the non-hydrodynamic mode damping rate to the study of hydrodynamics in the quark-gluon plasma. We further suggest that careful selection of initial conditions will make it possible to maximize the ratio $e^{-\Gamma_1 \bar{t}}/e^{-\Gamma_0 \bar{t}}$ and may enable the value of Γ_1 to be extracted with higher precision. We intend to explore these improvements in future work.

By fairly simple extensions of our hydrodynamic simulations, we intend to reproduce similar studies of collective oscillations in three dimensions. These studies will be applicable to a wider array of experimental data and therefore make the domain of applicability of our simulations more broad. Furthermore, hydrodynamics is a fundamentally different theory in two dimensions than three, and in quantum fluids in particular quantum fluctuations play a much larger role in two dimensions than in three [20]. We therefore expect that simple extensions of our simulations to three dimensions may yield new physical insight.

Further possibilities for improvements to the accuracy of the simulation would be tests of the spatially-constant temperature profile assumed in the simulations of collective oscillations, and possible improvements to the stability of the spatially-dependent temperature model that would enable us to implement this in the code.

We finally note that the primary motivation of this work is not the results presented in this thesis, but to verify the accuracy and stability of the code in several different physical configurations so that it may be used later to study new physics which has not yet been produced in the laboratory and suggest avenues to experimentalists which may yield interesting new results. Some ideas which we have discussed so far with collaborators Ana Maria Rey and the group of Deborah Jin involve using our code to study spin diffusion in unitary Fermi gases. Our hydrodynamic description also remains valid near the unitary regime but where the scattering length a is effectively finite, and we may use our code to study the behavior of the transport coefficients and the equation of state of the Fermi gas through the crossover regime. We note that the parameter τ_E which characterizes the relaxation to equilibrium of the internal energy distribution function $\epsilon(\mathbf{x}, \mathbf{v}, t)$ in Eq. (4.1) also corresponds (as its analog for the particle distribution function $f(\mathbf{x}, \mathbf{v}, t)$ does to the shear

viscosity) to a transport coefficient called the thermal conductivity which may also be interesting to study in the crossover regime. We also note that our approach is not specific to cold atomic gases of fermions and may be used to study the crossover regime in Bose gases.

Bibliography

[1] Jasmine Brewer, M. Mendoza, R.E. Young, and Paul Romatschke. Lattice boltzmann simulations of a two-dimensional fermi gas at unitarity. In preparation.

[2] Tetsufumi Hirano and Yasushi Nara. Eccentricity fluctuation effects on elliptic flow in relativistic heavy ion collisions. arXiv:0904.4080v1, 2009.

[3] D. J. Dean and M. Hjorth-Jensen. Pairing in nuclear systems: from neutron stars to finite nuclei. arXiv:0210033, 2002.

[4] Sadamichi Maekawa and Masatoshi Sato. Physics of High-Temperature Superconductors. Springer, 1992.

[5] T. Schäfer. What atomic liquids can teach us about quark liquids. Progress of Theoretical Physics, Supplement 168, 2007.

[6] R. Baier, P. Romatschke, D. T. Son, A. O. Starinets, and M. A. Stephanov. Relativistic viscous hydrodynamics, conformal invariance, and holography. Journal of High Energy Physics, 04:100, 2008.

[7] P. Kovtun, D.T. Son, and A.O. Starinets. Viscosity in strongly interacting quantum field theories from black hole physics. Phys. Rev. Lett., pages 94, 111601, 2005.

[8] Thomas Schäfer. Shear viscosity and damping of collective modes in a two-dimensional fermi gas. arXiv:1111.7242v2, 2012.

[9] Jonas Lätt. Hydrodynamic limit of lattice Boltzmann equations. PhD thesis, University of Geneva, 2007.

[10] Shiyi Chen and Gary D. Doolen. Lattice boltzmann method for fluid flows. Annu. Rev. Fluid Mech., 30:329–364, 1998.

[11] K. Dusling and T. Schäfer. Elliptic flow of the dilute fermi gas: From kinetics to hydrodynamics. Phys. Rev. A, 84:013622, 2011.

[12] P. Romatschke, M. Mendoza, and S. Succi. A fully relativistic lattice boltzmann algorithm. Phys. Rev. C, 84:034903, 2011.

[13] M. H. Anderson, J. R. Ensher, M. R. Matthews, C. E. Wieman, and E. A. Cornell. Observation of bose-einstein condensation in a dilute atomic vapor. Science, 198:269, 1995.

[14] B. DeMarco and D. S. Jin. Onset of fermi degeneracy in a trapped atomic gas. Science, 1703:285, 1999.

[15] Bernd Fröhlich. A Strongly Interacting Two-Dimensional Fermi Gas. PhD thesis, University of Cambridge, 2011.

[16] Cindy Regal. Experimental realization of BCS-BEC crossover physics with a Fermi gas of atoms. PhD thesis, University of Colorado at Boulder, 2005.

[17] T. Schäfer and C. Chafin. Scaling flows and dissipation in the dilute fermi gas at unitarity. arXiv:0912.4236v3, 2010.

[18] Riedl et al. Collective oscillations of a fermi gas in the unitarity limit: Temperature effects and the role of pair correlations. Phys. Rev. A, page 78, 2008.

[19] E. Vogt, M. Feld, B. Fröhlich, D. Pertot, M. Koschorreck, and M. Köhl. Scale invariance and viscosity of a two-dimensional fermi gas. arXiv:1111.1173v2, 2012.

[20] M. Bauer, M. Parish, and T. Enss. Universal equation of state and pseudogap in the two-dimensional fermi gas. arXiv:1311.1000v2, 2014.

[21] He, Chen, and Doolen. A novel thermal model for the lattice boltzmann method in incompressible limit. Journal of Computational Physics, 146:282–300, 1998.

[22] S. Kondaraju, H. Farhat, and J.S. Lee. Study of aggregational characteristics of emulsions on their rheological properties using the lattice boltzmann approach. Soft Matter, 8:1374–1384, 2012.